Atmospheric Research 277 (2022) 106307

Contents lists available at ScienceDirect

Atmospheric Research

journal homepage: www.elsevier.com/locate/atmosres

Linkage of extreme temperature change with atmospheric and locally anthropogenic factors in China mainland

Siqi Zhang [a,b], Guoyu Ren [a,b,*], Yuyu Ren [b], Suonam KealdrupTysa [a]

[a] Department of Atmospheric Science, School of Environmental Studies, China University of Geosciences (CUG), Wuhan 430074, China
[b] Laboratory for Climate Studies, National Climate Center, China Meteorological Administration (CMA), China

ARTICLE INFO

Keywords:
Extreme temperature
Climate change
Surface solar radiation
Cloud cover
Water vapor
Urbanization effect
China mainland

ABSTRACT

Much attention has been given to the large-scale anthropogenic influence on extreme temperature changes. However, the possible effects of atmospheric factors and the role of the locally anthropogenic driver on the observed regional change in extreme temperatures have not been well understood. Datasets of the China Meteorological Administration (CMA) were used to examine the possible influence. The data include the homogenized surface air maximum/minimum temperature, surface sunshine duration (*SSD*), water vapor pressure (*VAP*), and total cloud cover (*CLO*) during 1961–2020. We calculated the seasonal means of maximum temperature ($Tx_{(mean)}$), minimum temperature ($Tn_{(mean)}$) and diurnal temperature range (*DTR*) to analyze the characteristics of extreme surface air temperature (*ESAT*) changes in winter and summer, and their relationship to *SSD, VAP*, and *CLO*, as well as the urbanization effect in the extreme temperature indices series. The changes in the trends for *SSD* and *VAP* were more closely correlated with *ESAT* in winter and summer, respectively. The decreasing of *SSD* led to a slowing of the *ESAT* warming, while an increase of the *VAP* led to the intensification of *ESAT* warming. In addition, *CLO* also had an important role in the change of *ESAT*. The seasonal mean correlation coefficient over China mainland between $Tn_{(mean)}$ and *VAP* were statistically significant and higher than those with *SSD* and *CLO*. The seasonal mean correlation between $Tx_{(mean)}$/*DTR* and *SSD* were also statistically significant. The *SSD* and *VAP* strongly influenced the $Tx_{(mean)}$ in winter. The urbanization contribution to the *DTR* trends reached >25% in both winter and summer. *SSD* strongly influenced the trend of *ESAT* in urban area whereas *CLO*/*VAP* had larger influence on the trend of *ESAT* in rural area, which were all related to the urbanization effect as observed in the data series.

1. Introduction

Global warming has accelerated since the late 1970s (Jones et al., 2012; Hartmann et al., 2013; Sun et al., 2017; IPCC, 2021). This accelerated warming has also led to significant changes in the intensity, frequency, seasonality, and spatial distribution characteristics of climate variables including temperature, humidity, wind, and snow (IPCC, 2021). Among these, global and regional extreme surface air temperatures (*ESAT*) have received significant attention and have become important metrics in monitoring and studies of climate change (Nicholls and Alexander, 2007; Alexander et al., 2006; Donat et al., 2003; Kim et al., 2016; Yin and Sun, 2019; Zhai et al., 2021).

The study of *ESAT* for the both land on a global scale and most regions has indicated that the warming rate of the maximum temperatures was smaller than the warming of the minimum temperatures since the 1950s (Zhang et al., 2000; Zhai and Pan, 2003; Hundecha and Bárdossy, 2005; Makowski et al., 2009; Rio et al., 2012; Hartmann et al., 2013; Powell and Keim, 2014; Sun et al., 2017), with the warming rate of the minimum temperature being twice that of the maximum temperature, which had led to the significant decrease in the diurnal temperature range (*DTR*) (Alexander et al., 2006; Wang et al., 2014; Thorne et al., 2016; Sun et al., 2018). The accelerated warming of *ESAT* virtually had caused the hot extremes to become more frequent and more intense, whereas cold extremes (including cold waves) are becoming less frequent and less intense (IPCC, 2021). Therefore, more attention should be given to the seasonal *ESAT*, especially to the extreme low temperatures in winter and extreme high temperatures in summer.

Many studies have pointed out that on a global and regional scale for land, *ESAT* trends were related to multi-decadal natural variability along with anthropogenic factors such as the increased concentration of

* Corresponding author at: Department of Atmospheric Science, School of Environmental Studies, China University of Geosciences (CUG), Wuhan 430074, China.
E-mail address: guoyoo@cma.cn (G. Ren).

https://doi.org/10.1016/j.atmosres.2022.106307
Received 25 April 2022; Received in revised form 13 June 2022; Accepted 13 June 2022
Available online 18 June 2022

atmospheric CO_2 and aerosols, and some atmospheric factors such as solar radiation, cloud cover, and water vapor (Dai et al., 1999; Wang et al., 2010). Solar radiation as a general heat source was considered the root cause of the temperature change. Researchers (Wild, 2012; Yang et al., 2013; Wang et al., 2014) have pointed out that the temporal and spatial patterns of global *ESAT* change were consistent with the trends in radiation characteristics. Cloud cover had a strong influence on the amount of solar radiation reaching the ground. Dai et al. (1997), Croke et al. (1999) and Liu et al. (2016) indicated that a significant negative correlation existed between cloud cover and the amount of radiation received by the ground in most regions of the world. Moreover, aerosols in the atmosphere also acted as cloud condensation nuclei to increase the albedo of clouds, and also absorbed and scattered solar radiation to reduce the amount of radiation received at the ground (Wild, 2012; Liu et al., 2016). The circulation of water in the atmosphere and soil also affected the *ESAT*. The previous studies have shown that water vapor could increase surface temperatures as an important greenhouse gas (Stone and Weaver, 2003). The *DTR* decreased with an increase in precipitation rate, soil moisture, and water vapor (Dai et al., 1999; Zhao, 2014). Dai et al. (1999) believed that cloud cover was closely related to these factors and thus influenced the *DTR*. However, the robust association of long-term *ESAT* change with regional atmospheric factors still needs to be investigated.

Human activities have already affected global and regional changes in extreme weather and climate events, and the actuality of the human impacts was regarded almost certain in the recent International Panel on Climate Change report AR6 (IPCC, 2021). In contrast, urbanization, as a reflection of intense human activity at a local scale, was affirmed as an important factor influencing the observational changes in regional *ESAT* (Ren et al., 2007, 2008; Hua et al., 2008; Ren and Ren, 2011; Ren and Zhou, 2014). The urbanization not only directly affected the observed values of maximum/minimum temperatures and *DTR* by changing canopy radiation and energy balance (Ren and Zhou, 2014; Tysa et al., 2019; Sun et al., 2021; Zhang et al., 2021), but also affected the trends in cloud cover, water vapor, and aerosols (Romanov, 1999; Pielke et al., 2002; Hansen et al., 2005; Zhao et al., 2012; Sun et al., 2021; Yang et al., 2021). It is also obvious that, although urbanization effects on annual mean and extreme temperature trends in China had been analyzed, but the possible contribution of urbanization to winter and summer *ESAT* changes and atmospheric factors is still not quantified.

In this study, we first examined the characteristics of *ESAT* changes in winter and summer over China mainland, and the relationship of the trends between *ESAT* and three atmospheric factors (solar radiation, cloud cover, and water vapor). This will be able to compensate for the study on atmospheric factors affecting extreme temperature changes; we then evaluate the effects of urbanization on, and the contribution of urbanization to, the changes in *ESAT*, and solar radiation, cloud cover and water vapor in summer and winter over China mainland during 1961–2020; finally, we analyze the relationship of the trends in *ESAT* and three atmospheric factors aturban and rural stations in order to understand the possible effect of urbanization on seasonal extreme temperatures and atmospheric factors.

2. Data and method

2.1. Data and index definition

We used the *China Meteorological Administration-Surface Temperature daily dataset* (Cao et al., 2016), which has been quality-controlled and homogenized. The recorded length covers 70 years (1951–2020) and includes the daily maximum and minimum surface air temperatures (T_{max} and T_{min}, respectively). From the data, we calculated three *ESAT* values ($Tx_{(mean)}$, $Tn_{(mean)}$, and *DTR*). $Tx_{(mean)}$ and $Tn_{(mean)}$ were the seasonal means of T_{max} and T_{min}, while *DTR* was the difference between $Tx_{(mean)}$ and $Tn_{(mean)}$ (Klein Tank et al., 2009). In addition, we also used the *China Meteorological Administration-Surface Meteorological Elements monthly dataset*, which includes surface sunshine duration (*SSD*), water vapor pressure (*VAP*), and total cloud cover (*CLO*). This dataset has also been strictly quality controlled, and also has a recorded length of 70 years (1951–2020). The procedure of the quality control included threshold value check, extreme-value check, time consistency check, space consistency check, manual verification and correction. The correcting rates of *VAP*, *SSD* and *CLO* were about 0.99%, 1.98% and 0.03%, respectively. The discarding rate of *VAP* and *CLO* data was about 0.07‰. However, the cloud cover data had a larger missing rate and the significant inhomogeneity after 2015, mainly due to the transformation of observation from manual to automatic stations, but the time length was relatively short, and they would not significantly affect the analysis results.

2.2. Station classification

The *China Meteorological Administration-Surface Temperature daily dataset* and the *China Meteorological Administration-Surface Meteorological Elements monthly dataset* both include 2419 stations that are officially divided into three levels: The National Reference Climate Network (RCN), National Basic Meteorological Network (BMN), and National Ordinary Meteorological Network (OMN). In this study, we selected 825 stations (RCN and BMN) that were spatially evenly distributed across the country and have been widely used in related climate change monitoring and research. Owing to the sparseness of early year records during 1951–1961, in this study, we only used the data beginning in 1961. We also screened out the stations with a relatively high rate of missing records, according to the criteria of having at least 55 years of records in the whole period and at least 3 years of records for each of the analyzed decades. If the missing daily data reached 7 days in a month, the data of the entire month were regarded as missing. According to the above selection standards (China Meteorological Administration, 2003), a total of 770 national stations across mainland China in the period 1961–2020 were ultimately used in this study.

We used the data of these 770 national stations to calculate the three *ESAT* values and three natural factors for evaluating the impact of urbanization on trends of *ESAT*. The station classification was made by Tysa et al. (2019), which considered the proportions of land use/land cover in different buffer areas around the stations. Thus, data from 576 urban and 194 rural stations were obtained for data analysis. The selection of rural station networks also referred the previous study by Ren et al. (2010, 2015), which considered the need to be meet conditions of good continuity and integrity in the observational data, with less emphasis on the relocation of stations and the immunity of stations to the urbanization effect. The distributions of the urban and rural stations

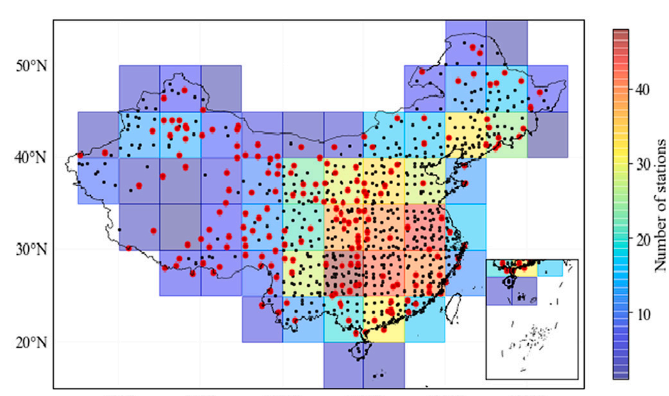

Fig. 1. Distribution of the 770 national weather stations used in this study. Black and red dots indicate urban and rural stations; the background color indicates number of stations for each grid box of 5° × 5° latitude and longitude. (For interpretation of the references to color in this figure legend, the reader is referred to the web version of this article.)

are shown in Fig. 1. The stations in northwestern Qinghai-Tibet Plateau were small in number, but stations in other regions had recorded data with good coverage.

2.3. Statistical methods

In this study, we selected winter (December to February) and summer (June to August) as the representative seasons. The seasonal *SSD* was the arithmetic sum of the monthly *SSD*. The seasonal mean *VAP* and *CLO* were calculated based on monthly mean values. The anomaly time series of *ESAT*, *SSD*, *VAP*, and *CLO* were calculated; the climate reference period was the 30 years of 1981–2010 in this study.

The temporal features, in particular the linear trend and the interannual variability, of the three *ESAT* indices, *SSD*, *VAP*, and *CLO* were analyzed in this study. The linear trend (*Tr*) is the regression coefficient was obtained by the least–squares method. *VA* means the variables of *ESAT* and atmospheric factors. *t* means the years and *n* means the number of each variables. [Eq. (1)]

$$Tr = \frac{\sum_{i=1}^{n} VA_i t_i - \frac{1}{n}\left(\sum_{i=1}^{n} VA_i\right)\left(\sum_{i=1}^{n} t_i\right)}{\sum_{i=1}^{n} t_i^2 - \frac{1}{n}\left(\sum_{i=1}^{n} t_i\right)^2} \quad (1)$$

The significance of correlations coefficient (*S*) for the climate trend represents the quantitative degree of temperature rise and fall under climate change, *VA*, *t* and *n* has the same meaning as Eq. (1) [Eq. (2)]. In examining the interannual variability, however, the linear trends of the *EAST* and atmospheric factors were removed.

$$S = \frac{\sum_{i=1}^{n}(VA_i - \overline{VA})(t_i - \overline{t})}{\sqrt{\sum_{i=1}^{n}(VA_i - \overline{VA})^2}\sqrt{\sum_{i=1}^{n}(t_i - \overline{t})^2}} \quad (2)$$

In addition, we used the area-weighted regional average method to calculate the regional average of all the indices and variables to evaluate the urbanization effect across mainland China. The calculation steps were as follow: 1) Each station across China was assigned to a 5° × 5° latitude–longitude grid box; then, the arithmetic average of all stations was calculated for each grid box. Fig. 1 shows the number of stations for each grid box. 2) The regional average over mainland China was calculated by applying the area-weighted method, which used the cosines of the mid-grid latitude as weights. The grid boxes with no stations (in northwestern Qinghai-Tibet Plateau) were not used for the calculation of a regional average.

The mean difference (*D*) for regional and each grid box between national stations and rural stations represents the average difference in the three *ESAT*, *SSD*, *VAP*, and *CLO* during 1961–2020. VA_{all} represents the variables of *ESAT* and atmospheric factors for national weather stations (urban and rural stations), VA_{rural} represented the variables of *ESAT* and atmospheric factors for rural stations [Eq. (3)]:

$$D = \sum_{i=1}^{n}\left(VA_{all(i)} - VA_{rural(i)}\right) \quad (3)$$

The linear trend of *D* value was urbanization effect. If the urbanization effect was significant, we calculated the urbanization contribution (*Co*) which was calculated by using Eq. (4) (Ren and Zhou, 2014):

$$Co = \frac{|(Tr_{all} - Tr_{rural})|}{Tr_{all}} * 100\% \quad (4)$$

where Tr_{all} represents the linear trends of national weather stations (urban and rural stations) for region and each grid box, and Tr_{rural} represented the linear trends of rural stations for each region and each grid box. If $(Tr_{all} - Tr_{rural}) > 0$ or $(Tr_{all} - Tr_{rural}) < 0$, this means urbanization had a positive or negative effect, respectively, on the trend of the climate variable or index.

3. Results

3.1. Temporal and the change of linear trends

The anomaly time series of *ESAT*, *SSD*, *VAP*, and *CLO* are shown in Fig. 2. The variables $Tx_{(mean)}$ and $Tn_{(mean)}$, experienced remarkable warming in 1961–2020. Initially, $Tx_{(mean)}$ cooled before 1985 and then warmed rapidly later, while $Tn_{(mean)}$ cooled before 1970 but warmed rapidly later (Fig. 2a–b). Because the warming rate of $Tx_{(mean)}$ was smaller than that of $Tn_{(mean)}$, *DTR* significantly decreased in 1961–2020. The variation of $Tx_{(mean)}$, $Tn_{(mean)}$, and *DTR* in winter were larger than those in summer. The *SSD* decreased but *VAP* increased during 1961–2020. The *CLO* increased in winter and decreased in summer. The variations of *SSD* and *CLO* in winter were larger than those in summer, whereas measurement of *VAP* in summer were larger than those in winter (Fig. 2d–f).

The box plots of linear trends for *ESAT*, *SSD*, *VAP*, and *CLO* in 1961–2020 shows that there were significant upward trends ($p < 0.05$) for $Tx_{(mean)}$, $Tn_{(mean)}$, *VAP*, and significant downward trends ($p < 0.05$) for *DTR* and *SSD* over most parts of mainland China. According to Fig. 3a&c, the average trends of $Tx_{(mean)}$ and $Tn_{(mean)}$ in winter were higher than those in summer, and those of *DTR* in winter were lower than those in summer. The trends of *VAP* in summer were more significant than those in winter. The average trends of *SSD* in summer were lower than those in winter (Fig. 3b&d). The spatial distributions for $Tx_{(mean)}$ and $Tn_{(mean)}$ showed that significantly upward trends existed in most parts of China, and weakly downward trends were observed in parts of southern, northeastern, and east-central China (Fig. 3a&c). The weak downward trends for $Tx_{(mean)}$ may be closely related to decreasing trends of *VAP* (in summer) and *SSD* in southern China. The warming trends for $Tx_{(mean)}$ and $Tn_{(mean)}$ in northern China were higher than those in southern China, which may be related to significantly upward trends and downward trends for *CLO* in most parts of northern and southern China, respectively (Fig. 3b&d). The warming trends of most of stations for $Tn_{(mean)}$ were higher than those for $Tx_{(mean)}$, resulting in the significantly downward trends for *DTR* over most parts of China.

Fig. 4 shows the relationship of the linear trends between *ESAT* and atmospheric factors *(VAP, SSD,* and *CLO)* in 1961–2020. Fig. 4a showed the trends of *SSD* were increased with the trends of $Tx_{(mean)}$ increasing and the change of trend for *SSD* was closely correlated ($r = 0.7$) with $Tx_{(mean)}$. The trends of *CLO* were decreased with the trends of $Tx_{(mean)}$ increasing and the change of trend for *CLO* was negative correlated ($r = -0.86$) with $Tx_{(mean)}$. The change of trend between *VAP* and *Tx(mean)* was no significant correlation. In general, the change of trend for *VAP* was closely correlated ($p < 0.05$) with $Tx_{(mean)}$ and *DTR* in summer (Fig. 4d&f). The change of trend for *SSD* was closely correlated ($p < 0.05$) with $Tx_{(mean)}$, $Tn_{(mean)}$, and *DTR* in winter (Fig. 4a–c). The change of trend for *CLO* was closely correlated ($p < 0.05$) with $Tx_{(mean)}$ in winter (Fig. 4a). These findings indicate the weakly downward trends for $Tx_{(mean)}$ were closely related to decreasing trends of *VAP* and *SSD* in summer and in winter, and closely related to decreasing trends of *CLO* and *SSD* in southern China. Thus, the changes in the trends for *SSD* and *VAP* were more closely correlated with *ESAT* in winter and summer, respectively. The decreasing trend of *SSD* led to a slowdown of *ESAT* warming, while the increasing of *VAP* led to the intensification of *ESAT* warming. In addition, *CLO* also had an important role in changes in *ESAT*.

3.2. Similarity of inter-annual to decadal variability

Fig. 5 shows the relationship of the detrended anomaly between extreme surface air temperature and atmospheric factors. Fig. 5a showed the detrended anomaly of *VAP/SSD* were increased with the detrended anomaly of $Tx_{(mean)}$ increasing and the change of detrended anomaly for *VAP/SSD* was closely correlated ($r = 0.80/\ r = 0.56$) with $Tx_{(mean)}$. The detrended anomaly of *CLO* were decreased with the

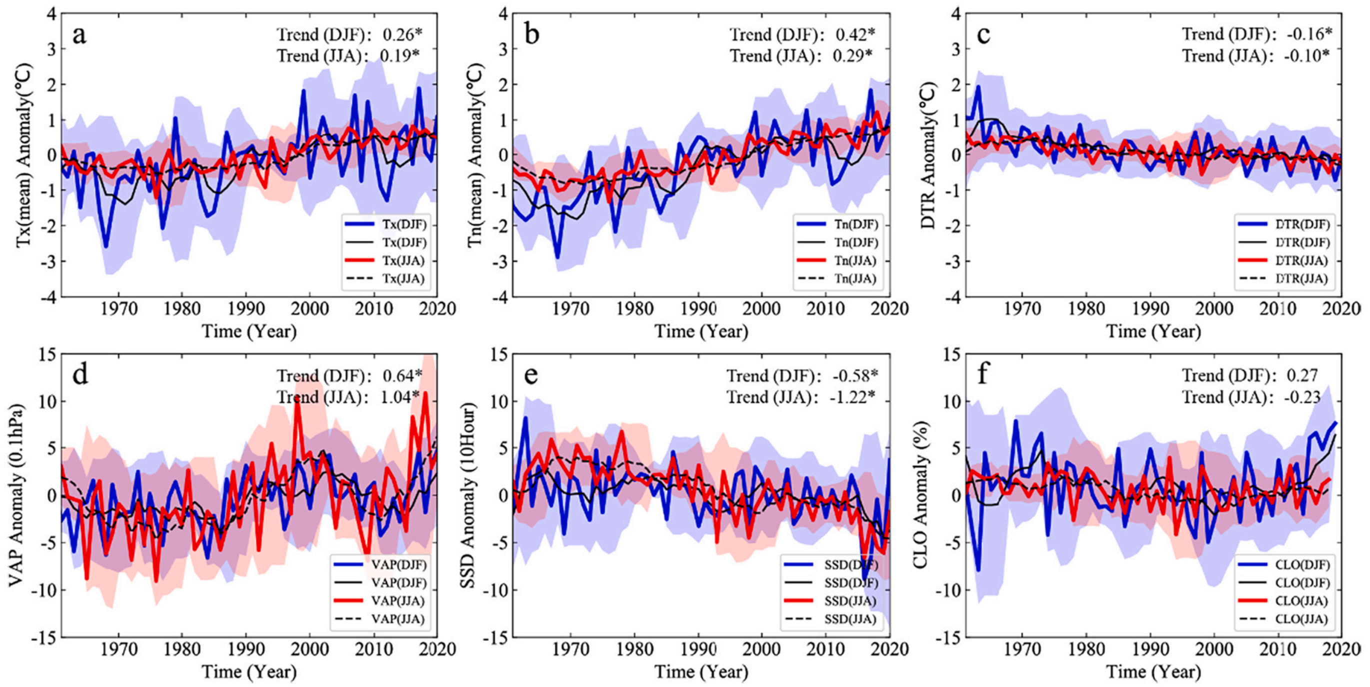

Fig. 2. Anomaly time series of extreme surface air temperature (*ESAT*) [(a) maximum temperature ($Tx_{(mean)}$), (b) minimum temperature ($Tn_{(mean)}$), (c) diurnal temperate range (*DTR*)] and atmospheric factors [(d) water vapor pressure (*VAP*), (e) surface sunshine duration (*SSD*), (f) total cloud cover (*CLO*)] in winter (DJF) and summer (JJA) over China during 1961–2020. The black lines represent a 5-year moving average, the shaded parts represent the standard deviation range of each time series and statistical significance ($p < 0.05$). The units of the trends are °C/10a for $Tx_{(mean)}$, $Tn_{(mean)}$ and *DTR,* 0.1 hPa/10a for *VAP,* 10 h/10a for *SSD*, and %/10a for *CLO*. * represent statistical significance ($p < 0.05$) for linear trends.

detrended anomaly of $Tx_{(mean)}$ increasing and the change of detrended anomaly for *CLO* was negative correlated ($r = -0.58$) with $Tx_{(mean)}$. In general, the changes in *VAP* were more significant than those of *SSD* and *CLO*, as can be seen in the remarkable increase for *VAP* from cold to warm detrended anomaly in $Tx_{(mean)}$ and $Tn_{(mean)}$ and the decreasing trend from cold to warm in *DTR*. The change in *SSD* and *CLO* from cold to warm detrended anomalies in $Tx_{(mean)}$ and *DTR* was more significant than that in $Tn_{(mean)}$, which increased remarkably for the *SSD* and decreased remarkably for *CLO*. This phenomenon indicated that the change of *VAP* was closely related to $Tx_{(mean)}$ and $Tn_{(mean)}$. The changes in *SSD* were more sensitive to $Tx_{(mean)}$ and *DTR*. In addition, *CLO* was negatively related to *ESAT*.

The correlation coefficients between the detrended anomaly series of *ESAT* and atmospheric factors (*SSD*, *VAP*, and *CLO*) acquired at the 770 stations show the similarity of the indices and factors in inter-annual and inter-decadal variability in 1961–2020 (Fig. 6). The color lines represent the sorted 770 stations from lowest to highest correlation coefficient for the detrended anomaly between *ESAT* and atmospheric factors separately. The box plots represent the correlation coefficient of 770 stations for the detrended anomaly between *ESAT* and atmospheric factors separately. The seasonal mean correlation coefficients over China between $Tn_{(mean)}$ and *VAP* were statistically significant ($p < 0.05$), which were higher than those of *SSD* and *CLO* with $Tn_{(mean)}$ (Fig. 6b&e). The seasonal mean correlation coefficients between $Tx_{(mean)}$/*DTR* and *SSD* were statistically significant ($p < 0.05$) and those between $Tx_{(mean)}$/*DTR* and *CLO* were negatively statistically significant ($p < 0.05$) (Fig. 6a,c,d, f). The correlation coefficient of 770 stations revealed similar characteristics with the seasonal mean correlation coefficient over China, which indicated that the change of *VAP* as a greenhouse gas was closely related to $Tx_{(mean)}$, $Tn_{(mean)}$, and *SSD* as a general heat source was considered to be positively related to $Tx_{(mean)}$ and *DTR*. In addition, *CLO* was negatively related to the $Tx_{(mean)}$ and *DTR*.

To analyze the regional characteristic of correction coefficients in 1961–2020, Fig. 7 shows the most relevant factors of seasonal variability for the detrended anomaly between *ESAT* and atmospheric factors (*SSD*, *VAP*, and *CLO*). Firstly, we calculated correlation coefficient for the detrended anomaly of each station between *ESAT* and atmospheric factors, respectively. Then we selected the maximum correlation coefficient for each station from the calculated correlation coefficient in first step and showed them in the Fig. 7. These shows which atmospheric factor was most associated with *ESAT*. The Fig. 7a&d showed the correction coefficients between *SSD* and $Tx_{(mean)}$ were higher than those of *VAP* and *CLO* in most of China except in north China, parts of the south China, and the coastal regions in winter, where the $Tx_{(mean)}$ was closely related to *VAP*. The $Tn_{(mean)}$ had the highest correlation coefficient with *VAP* except in part of southern and western China in summer, where the $Tn_{(mean)}$ had the highest correlation coefficient with *SSD* and *CLO* (Fig. 7b&e). The *DTR* was directly related to *SSD*, while *CLO* and *VAP* also played an important role in northern China and other parts of China. In addition, the correlation coefficient between *ESAT* and atmospheric factors (*SSD*, *VAP*, and *CLO*) were non-significant in some parts of northern, central, and western China.

3.3. Urbanization effect

Fig. 8 and Table 1 show the difference in the anomaly time series between national and rural stations over China and the effects of construction and urbanization on environmental conditions. For example, $Tn_{(mean)}$ experienced remarkable warming in 1961–2020, while *DTR* significantly decreased in 1961–2020. The change in $Tx_{(mean)}$ was unremarkable. The contributions of urbanization to $Tn_{(mean)}$ were higher than those of $Tx_{(mean)}$. The contributions of urbanization to *DTR* were >25% in winter and summer. These results were consistent with the conclusions by Zhang et al. (2010), Tysa et al. (2019), and Sun et al. (2021). All of these studies showed the increase of all-rural $Tx_{(mean)}$ difference series was much less than that of all-rural $Tn_{(mean)}$ difference series. Therefore, the annual and seasonal mean all-rural *DTR* difference series had a highly significant decreasing trend. Besides, as the

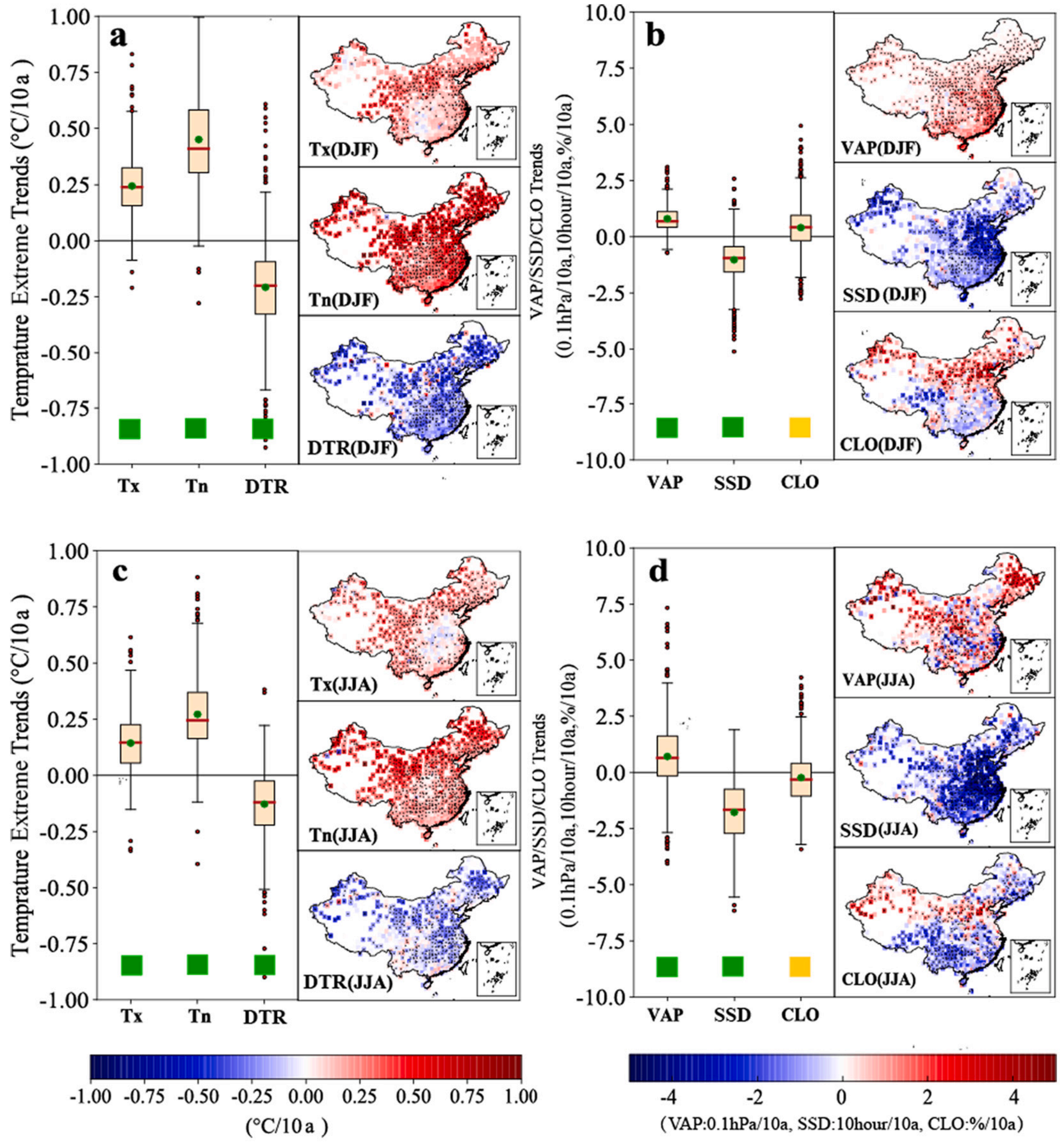

Fig. 3. Box plots and spatial distributions of linear trends for extreme surface air temperatures (*ESAT*) [maximum temperature ($Tx_{(mean)}$), minimum temperature ($Tn_{(mean)}$), diurnal temperate range (*DTR*)] and atmospheric factors [water vapor pressure (*VAP*), surface sunshine duration (*SSD*), total cloud cover (*CLO*)] in winter (a–b) and summer (c–d) at 770 stations during 1961–2020. Green dots and red lines represent the average of linear trends over China and the median of linear trends for 770 stations, respectively; green and yellow squares in the box figures represent statistically significance ($p < 0.05$) and insignificance ($p > 0.05$), respectively; black dots in spatial distribution represent statistical significance ($p < 0.05$). (For interpretation of the references to color in this figure legend, the reader is referred to the web version of this article.)

urbanization level increases, the urbanization effect on the *DTR* trends of the urban stations gradually increases. Urbanization also contributed to the increasing trend (positive urbanization effect) of cloud cover and water vapor (in winter) and the decreasing trend (negative urbanization effect) of water vapor (in summer) and radiation at the urban stations (Fig. 8d−f). Table 1 shows that the contribution of urbanization on *VAP* was 13.8% in winter and 24.2% in summer. The contribution of urbanization to *SSD* in winter (29.4%) was higher than that in summer (11.9%). The contribution of urbanization to *CLO* was 40.6% in winter and 38.1% in summer.

Fig. 9 shows the spatial distribution of urbanization effect and contribution of urbanization for *ESAT* and atmospheric factors. The urbanization effect on $Tx_{(mean)}$ and $Tn_{(mean)}$ in most of central China were more significant than those in other areas. Urbanization had a significant negative effect on *DTR* in most regions of China (Fig. 9a−f), leading to a significant decrease in seasonal mean *DTR* and intra-seasonal differences in extreme temperatures. The urbanization effect on *VAP* in most of southern China was negative and was more significant in southern China than in other areas (Fig. 9g&j). The urbanization effect on *SSD* in most of China was negative and was more significant in winter than in summer. In addition, urbanization had a significant impact on the chance in the observed *CLO* at most urban stations in the entire span of mainland China in winter and in central and eastern China in summer (Fig. 9i&l).

Table 2 shows the correlations coefficient of linear trend between regional average *ESAT* and atmospheric factors in winter and summer at urban and rural stations separately during 1961–2020 (Refer to Fig. 4 for calculation method of correlation coefficient). The correlation coefficient between *ESAT* and *SSD* were more significant in urban stations than rural stations, especially in wintertime, whereas the correlation coefficient between *ESAT* and *CLO/VAP* were more significant in rural stations than urban stations. The trend of *SSD* may have strongly influenced on the trend of *ESAT* in urban area, but the trend of *CLO/VAP* may have more significantly influenced the trend of *ESAT* in rural area.

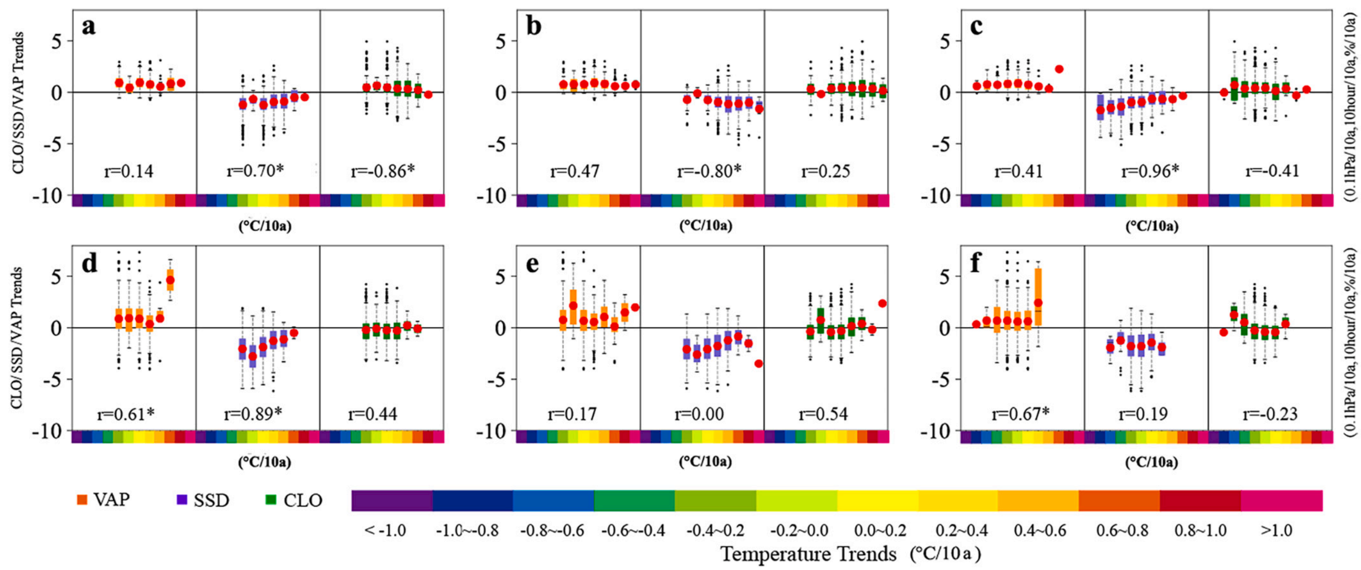

Fig. 4. Relationship of linear trends between extreme surface air temperatures (*ESAT*) [maximum temperature ($Tx_{(mean)}$, a, d), minimum temperature ($Tn_{(mean)}$, b, e), diurnal temperate range (*DTR*, c, f)] and atmospheric factors [water vapor pressure (*VAP*), surface sunshine duration (*SSD*), total cloud cover (*CLO*)] in winter (a–c) and summer (d–f) at 770 stations during 1961–2020. The color bar indicates the change of temperature trends from low to high temperature. The box diagrams show the trends characteristics of *SSD*, *VAP*, and *CLO* for national weather stations within each change of temperature trends; *r* shows the correlation between the average trends of *ESAT* and atmospheric factors, and * represents statistical significance ($p < 0.05$).

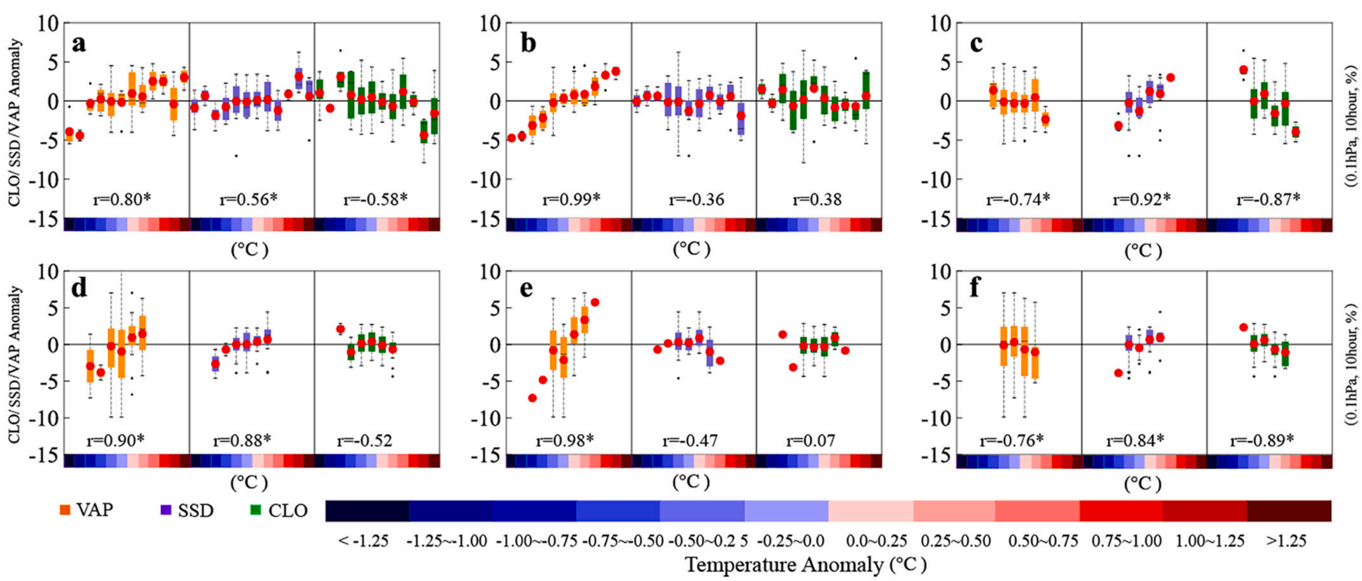

Fig. 5. Relationship of the detrended anomaly between extreme surface air temperature (*ESAT*) [maximum temperature ($Tx_{(mean)}$, a, d), minimum temperature ($Tn_{(mean)}$, b, e), and diurnal temperate range (*DTR*, c, f)] and atmospheric factors [water vapor pressure (*VAP*), surface sunshine duration (*SSD*), total cloud cover (*CLO*)] in winter (a–c) and summer (d–f) at 770 stations during 1961–2020. The color bar means the change of the detrended *ESAT* anomaly from low to high values. The box diagrams show the detrended anomaly characteristics of atmospheric factors for national weather stations within each change of temperature detrended anomaly; *r* showed the correlation between the average detrended anomaly of *ESAT* and atmospheric factors, and * represents statistical significance ($p < 0.05$).

The difference indicates that urbanization may have exerted an influence on the linear trends of *ESAT* and atmospheric factor at the urban stations.

4. Discussion

This article examined change of *ESAT* and its link with climatic factors, and the locally anthropogenic urbanization effects on the observed trends of *ESAT*, in China mainland. *VAP, SSD*, and *CLO,* as the important atmospheric factors, were involved in the atmospheric interaction and they jointly affected the change in extreme temperature (Fig. 10). Solar radiation as a general heat source was considered to be the root cause of the temperature change (Wild, 2012; Yang et al., 2013). The influence of solar radiation on the maximum temperature (daytime) is greater than the minimum temperature (nighttime), which had led to the significant impact on *DTR* (Alexander et al., 2006; Wang et al., 2014; Thorne et al., 2016; Sun et al., 2018). Thus, the decreasing solar radiation directly led to a slowdown of maximum temperature increase and downward trend of *DTR*. Cloud cover absorbs and scatters solar radiation, which reduces the amount of radiation received at the ground level

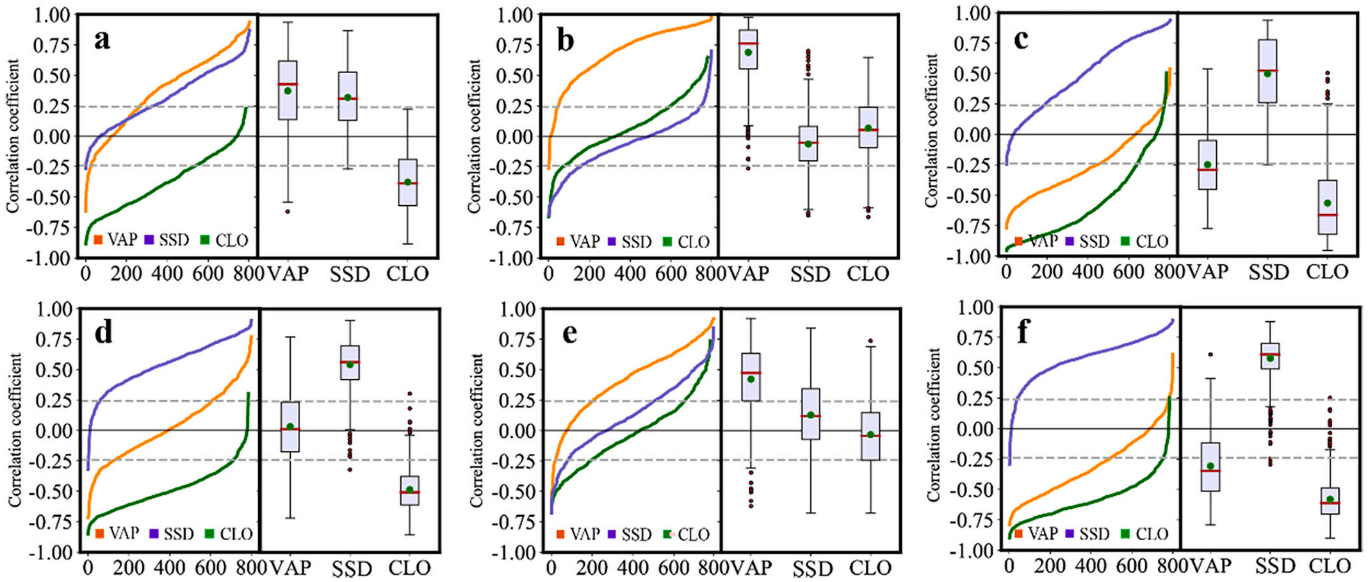

Fig. 6. Correlation coefficient of 770 stations for the detrended anomaly between extreme surface air temperature (*ESAT*) [[maximum temperature ($Tx_{(mean)}$, a, d), minimum temperature ($Tn_{(mean)}$, b, e), diurnal temperate range (*DTR*, c, f)] and atmospheric factors [water vapor pressure (*VAP*), surface sunshine duration (*SSD*), and total cloud cover (*CLO*)] in winter (a–c) and summer (d–f) over China during 1961–2020. Statistically significant ($p < 0.05$) trends are marked with an imaginary line; green dots and red lines in boxes represent the average of correlation coefficient over China and the median of correlation coefficient for 770 stations, respectively. (For interpretation of the references to color in this figure legend, the reader is referred to the web version of this article.)

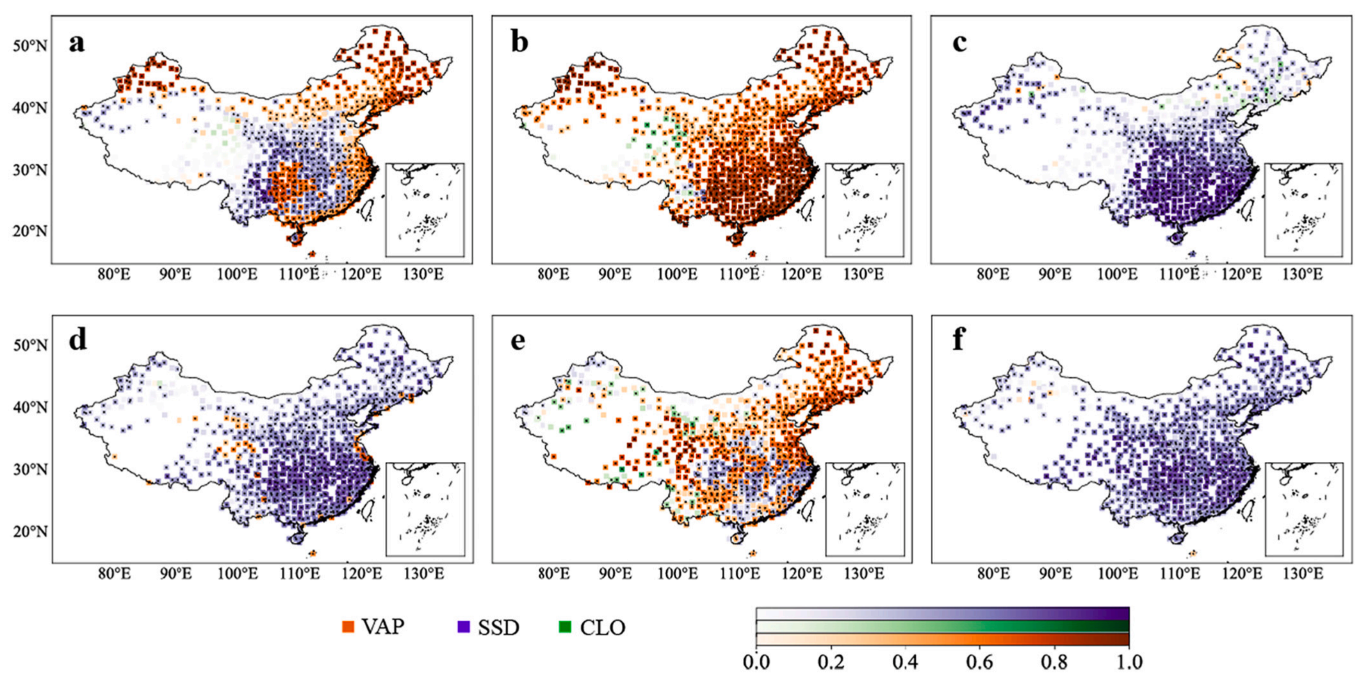

Fig. 7. Composite map of spatial maximum correlation coefficient for the detrended anomaly between extreme surface air temperature (*ESAT*) [[maximum temperature ($Tx_{(mean)}$, a, d), minimum temperature ($Tn_{(mean)}$, b, e), diurnal temperate range (*DTR*, c, f)] and atmospheric factors [water vapor pressure (*VAP*), surface sunshine duration (*SSD*), and total cloud cover (*CLO*)] in winter (a–c) and summer (d–f) over China during 1961–2020. The black dots represent statistical significance ($p < 0.05$).

(Wild, 2012; Liu et al., 2016), indirectly affecting the change in mean and extreme temperature. The water vapor is an important greenhouse gas (Stone and Weaver, 2003) in the atmosphere, and it could also influence the formation of cloud cover and the solar radiation received at ground surface. Increase in water vapor is conductive to the increase in minimum temperature and decrease in maximum temperature, leading to a decline of *DTR*. Overall, this study thus shows that the change in solar radiation and water vapor had a stronger influence on the changes in *ESAT*. The cloud cover also influenced the trend of change in *ESAT* as another important factor.

Urbanization can affect changes in temperature at urban weather stations through the enhanced urban heat island (UHI) effect (Ren and Zhou, 2014). Zhang et al. (2010) indicated that the contribution of urbanization to the observed temperature trend at national weather stations in China was at least 27%. In this study, it was found that the contributions of urbanization to *DTR* trend were higher than 25% in

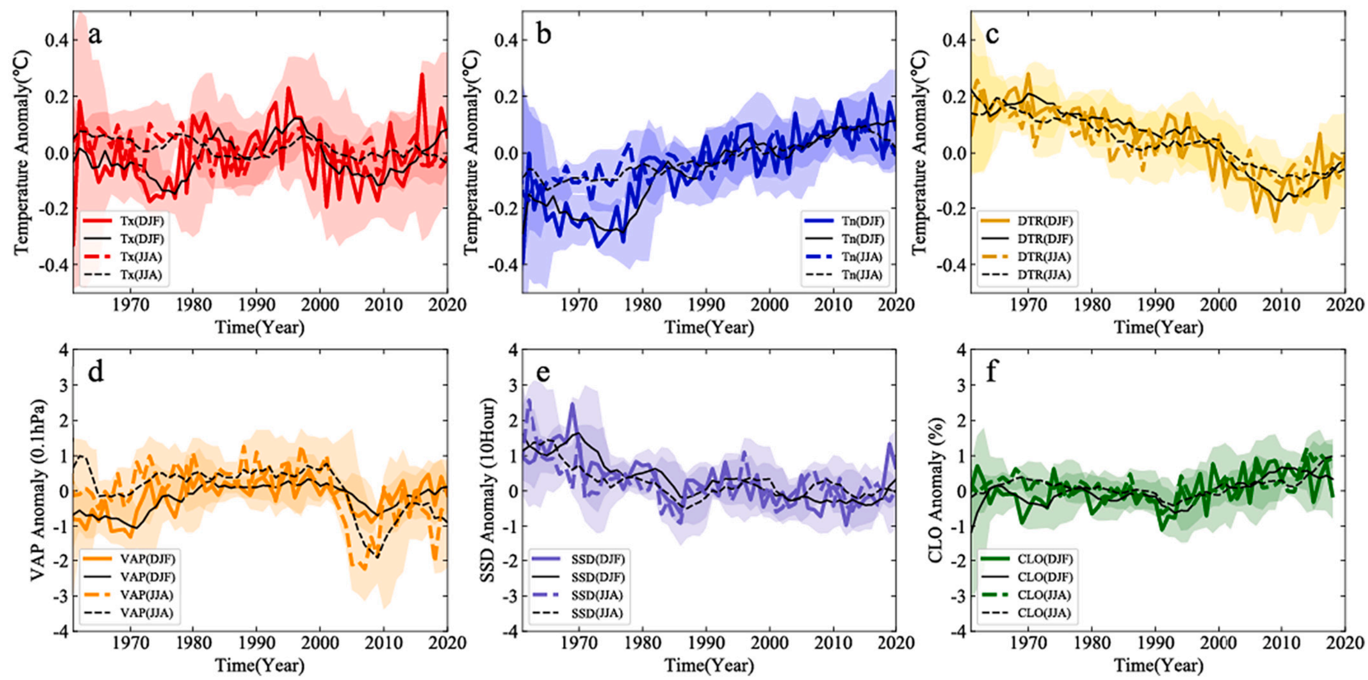

Fig. 8. Differences of anomaly time series between national stations and rural stations for extreme surface air temperature (*ESAT*) [(a) maximum temperature ($Tx_{(mean)}$), (b) minimum temperature ($Tn_{(mean)}$), (c) diurnal temperate range (*DTR*)] and atmospheric factors [(d) water vapor pressure (*VAP*), (e) surface sunshine duration (*SSD*), (f) total cloud cover (*CLO*)] in winter (DJF) and summer (JJA) over China during 1961–2020. The black lines represent the 5-year moving average; the shaded parts represent the standard deviation range of time series.

Table 1
Urbanization effect and contribution of urbanization in summer and winter over mainland China during 1961–2020 [N/A indicates that the urbanization effect was insignificant ($p > 0.05$)].

	Winter		Summer	
	Urbanization effect	Contribution of urbanization (%)	Urbanization effect	Contribution of urbanization (%)
$Tx_{(mean)}$	0.01	N/A	−0.01	N/A
$Tn_{(mean)}$	0.07	14.3	0.04	10.8
DTR	−0.06	26.9	−0.05	31.1
VAP	0.10	13.8	−0.20	24.2
SSD	−0.24	29.4	−0.16	11.9
CLO	0.11	40.6	0.06	38.1

Abbreviations: Extreme surface air temperature (*ESAT*) [$Tx_{(mean)}$ (°C/10a), $Tn_{(mean)}$ (°C/10a), and diurnal temperate range (*DTR*) (°C/10a)] and atmospheric factors [water vapor pressure (*VAP*) (0.1 hPa/10a), surface sunshine duration (*SSD*) (10 h/10a), and total cloud cover (*CLO*) (%/10a)].

winter and summer. In addition, the UHI effect also directly affected the atmospheric factors in different seasons (Table 1), which led to changes of *ESAT*. The effects of evapotranspiration and precipitation frequency in urban areas was smaller than in rural areas (Varquez and Kanda, 2018; Ren et al., 2021; Yang et al., 2021); meanwhile, lush vegetation, abundant irrigation, and frequent precipitation occurred in summer in rural areas, while the lack of lush vegetation and abundant irrigation in winter led to the contribution of urbanization to *VAP* being weaker in winter than in summer. Also, the city's complex three-dimensional structure also had increased the earth's albedo; also, the increase in winter air pollution and increased aerosol emissions caused by increasing of human activity resulted in a decrease in the solar radiation received at the earth's surface (IPCC, 2021; Arnfield, 2003). These factors led to the contribution of urbanization to *SSD* in winter being higher than that in summer. In addition, the contribution of urbanization to *CLO* was stronger than those of *SSD* and *VAP*; the reason for this may be that urbanization resulted in an increase in aerosol and water vapor emissions, which helped in cloud formation in winter; furthermore, the effects of evapotranspiration and precipitation frequency helped in cloud formation in rural areas in summer.

However, the cloud cover data also has some quality problems, which includes the absence of cloud cover data and the inhomogeneity of the time series after 2015. These problems were due to the change in methods of observation from manual to automatic station observation. Cloud cover data needs to be further quality controlled and homogenized in the future. Besides, there are also some limitations which would affect the analysis results. These include selection of the reference period and the varied numbers of stations in the same region. The difference of reference period might affect climate anomaly values of time series, but it will not affect the estimates of the trends. The different numbers of observation stations might have a slight impact on the results, although we used the area-weighted regional average method to construct the regional time series, which greatly reduced the error caused by the different number of stations. The spatial variation in number of stations might still have an effect on the robustness of the area-weighted averaging values for the station-sparse areas of western China.

5. Conclusions

The primary conclusions of this study are as follows:

1) The warming trends of $Tn_{(mean)}$ were higher than those of $Tx_{(mean)}$ in winter and summer across China, which had led directly to the decreasing trends for *DTR*. The change of trend for *SSD* and *VAP* were more closely correlated with the *ESAT* in winter and summer, respectively. The decreasing of *SSD* led to a slowdown of *ESAT* warming, while the increasing of *VAP* has led to an intensification of *ESAT* warming. In addition, *CLO* also had an important role in the changes in *ESAT*.
2) The seasonal mean correlation over China between $Tn_{(mean)}$ and *VAP* was statistically significant and higher than those of *SSD* and *CLO*. The seasonal mean correlation coefficient between *DTR* and *SSD* was

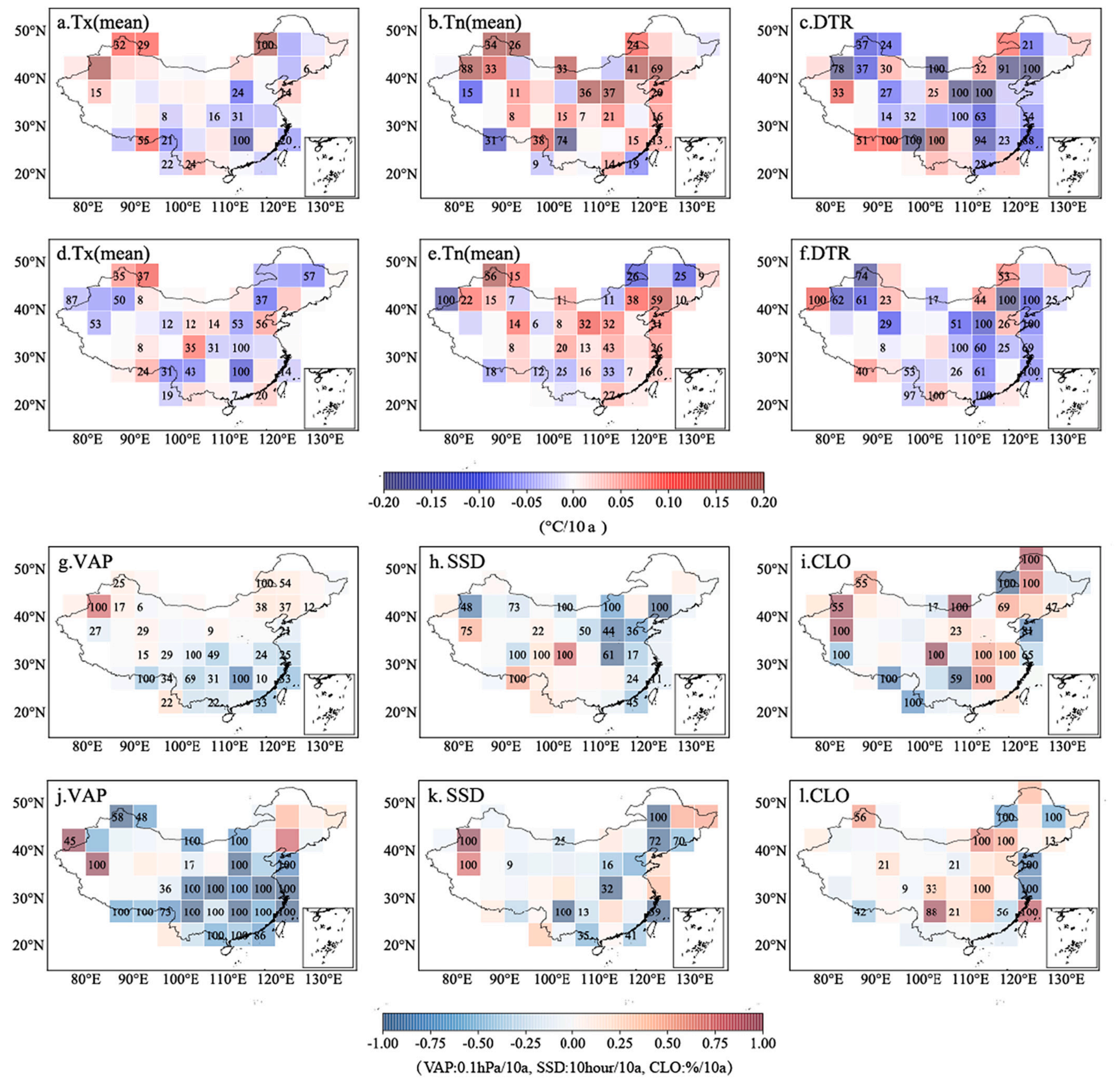

Fig. 9. Spatial distribution of urbanization effect for extreme surface air temperature (*ESAT*) [maximum temperature ($Tx_{(mean)}$, a, d), minimum temperature ($Tn_{(mean)}$, b, e), diurnal temperate range (*DTR*, c, f)] and atmospheric factors [water vapor pressure (*VAP*, g, j), surface sunshine duration (*SSD*, h, k), and total cloud cover (*CLO*, i, l)] in winter (a–c, g–i) and summer (d–f, j–l) over China during 1961–2020. The numbers represent statistical significance of urbanization contribution ($p < 0.05$).

Table 2
The correlations coefficient of linear trend between regional average extreme surface air temperatures (*ESAT*) and atmospheric factors in winter and summer at urban and rural stations during 1961–2020. [* indicates that the correlation coefficient was significant ($p < 0.05$)].

Region	Value	Winter			Summer		
		VAP	*SSD*	*CLO*	*VAP*	*SSD*	*CLO*
Urban	$Tx_{(mean)}$	0.02	0.80*	−0.22	−0.51	0.86*	0.39
	$Tn_{(mean)}$	−0.34	−0.85*	0.55*	−0.03	0.16	0.54
	DTR	−0.56*	0.97*	−0.39	0.58*	−0.53	−0.14
	$Tx_{(mean)}$	0.09	0.15	−0.89*	0.54	0.58*	0.45
	$Tn_{(mean)}$	−0.56*	−0.37	−0.67*	0.03	0.29	0.08
Rural	*DTR*	0.56*	0.38	0.27	0.71*	−0.29	0.67*

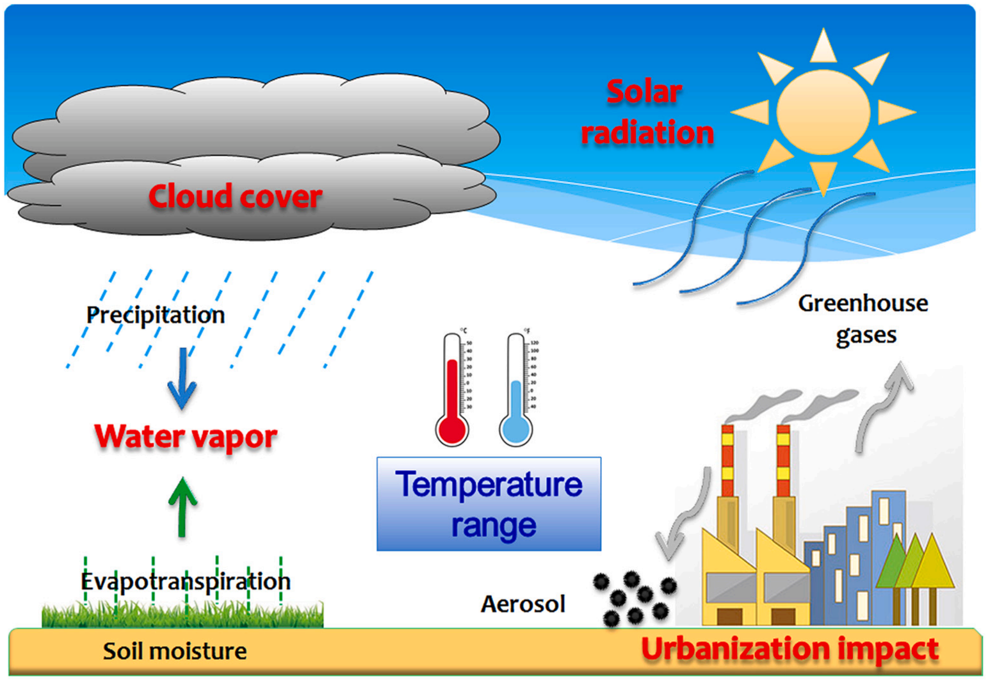

Fig. 10. Diagrammatic association of regional extreme temperature change with atmospheric and locally anthropogenic factors.

statistically significant and was also statistically significant for $Tx_{(mean)}$. The *SSD* and *VAP* had a strong influence on $Tx_{(mean)}$ in winter. The seasonal mean negative correlation coefficients over China between $Tx_{(mean)}/DTR$ and *CLO* were statistically significant.

3) Urbanization had a positive effect on *VAP* (13.8% in winter), *SSD* (29.4% in winter and 11.9% in summer), and *CLO* (40.6% in winter) and a negative effect on *VAP* (24.2% in summer) and *CLO* (38.1% in summer), which was directly related to the change of *ESAT*. The change of *SSD* strongly influenced the trend of *ESAT* in urban area whereas that of *CLO/VAP* had larger influence on the trend of *ESAT* in rural area, which caused the larger influence of urbanization on the trends of the solar radiation and water vapor/cloud cover, and in turn on the trends of *ESAT*. The results revealed that the impacts of urbanization on $Tn_{(mean)}$ were higher than those of $Tx_{(mean)}$. The contributions of urbanization to *DTR* trend were higher than 25% in winter and summer.

Author contributions statement

S.Z and G.R contributed the central idea, S.Z made all the calculations and analysis, Y.R carried out data analyses, S·K, Y.R and GR revised the manuscript.

Declaration of Competing Interest

The authors declared that they have no conflicts of interest to this work.

Acknowledgments

This study is financed by the National Key Research and Development Program of China (No. 2018YFA0605603, 2020YFA0608203), China Three Gorges Corporation (No. 0704181), The National Natural Science Foundation of China (42005036), the Science and Technology Program of Guangzhou (202102021188), and the Independent Research Project Program of State Key Laboratory of Tropical Oceanography (LTOZZ2102).

References

Alexander, L.V., Zhang, X.B., Peterson, T.C., Caesar, J., Vazquez-Aguirre, J.L., 2006. Global observed changes in daily climate extremes of temperature and precipitation. J. Geophys. Res.-Atmos. 111, 1042–1063. https://doi.org/10.1029/2005JD006290.

Arnfield, A.J., 2003. Two decades of urban climate research: a review of turbulence, exchanges of energy and water, and the urban heat island. Int. J. Climatol. 23, 1–26. https://doi.org/10.1002/joc.859.

Cao, L., Zhu, Y., Tang, G., Yuan, F., Yan, Z., 2016. Climatic warming in China according to a homogenized dataset from 2419 stations. Int. J. Climatol. 36, 4384–4392. https://doi.org/10.1002/joc.4639.

China Meteorological Administration, 2003. Specification for surface meteorological observation. China Meteorol. Press. 124p.

Croke, M.S., Cess, R.D., Hameed, S., 1999. Regional cloud cover change associated with global climate change: case studies for three regions of the United States. J. Clim. 12, 2128–2134. https://doi.org/10.1175/1520-0442(1999)0122.0.CO;2.

Dai, A., Genio, A., Fung, I.Y., 1997. Clouds, precipitation and temperature range. Nature. 386, 665–666. https://doi.org/10.1038/386665b0.

Dai, A., Trenberth, K.E., Karl, T.R., 1999. Effects of clouds, soil moisture, precipitation, and water vapor on diurnal temperature range. J. Clim. 12, 2451–2473. https://doi.org/10.1175/1520-0442(1999)0122.0.CO;2.

Donat, M.G., Alexander, L.V., Yang, H., 2003. Updated analyses of temperature and precipitation extreme indices since the beginning of the twentieth century: the HadEX2 dataset. J. Geophys. Res.-Atmos. 118, 2098–2118. https://doi.org/10.1002/jgrd.50150.

Hansen, J., Nazarenko, L., Ruedy, R., Sato, M., Tausnev, N., 2005. Climate change: earth's energy imbalance: confirmation and implications. Science. 308, 1431–1435. https://doi.org/10.1126/science.1110252.

Hartmann, D., Tank, A.K., Rusticucci, M., 2013. Observations: atmosphere and surface. In: Climate Change 2013: The Physical Science Basis. Contribution of Working Group I to the Fifth Assessment Report of the Intergovernmental Panel on Climate Change. Cambridge University Press, Cambridge, United Kingdom.

Hua, L.J., Ma, Z.G., Guo, W.D., 2008. The impact of urbanization on air temperature across China. Theor. Appl. Climatol. 93, 179–194. https://doi.org/10.1007/s00704-007-0339-8.

Hundecha, Y., Bárdossy, A., 2005. Trends in daily precipitation and temperature extremes across western Germany in the second half of the 20th century. Int. J. Climatol. 25, 1189–1202. https://doi.org/10.1002/joc.1182.

IPCC, 2021. Climate Change 2021: The Physical Science Basis. Cambridge University Press, Cambridge. https://www.ipcc.ch/report/ar6/wg1/#FullReport.

Jones, P.D., Lister, D.H., Osborn, T.J., Harpham, C., Salmon, M., Morice, C.P., 2012. Hemispheric and large-scale land-surface air temperature variations: an extensive revision and an update to 2010. J. Geophys. Res.-Atmos. 117 https://doi.org/10.1029/2011JD017139.

Kim, Y.H., Min, S.K., Zhang, X., Zwiers, F., Alexander, L.V., Donat, M.G., 2016. Attribution of extreme temperature changes during 1951–2010. Clim. Dyn. 46, 1769–1782. https://doi.org/10.1007/s00382-015-2674-2.

Klein Tank, A.M.G., Zwiers, F.W., Zhang, X., 2009. Guidelines on analysis of extremes in a changing climate in support of informed decisions for adaptation. In: Climate Data and Monitoring. WCDMP-No. 72. WMO-TD/No. 1500. Geneva, Switzerland, p. 49.

Liu, L., Li, Z., Yang, X., Gong, H., Li, C., Xiong, A., 2016. The long-term trend in the diurnal temperature range over Asia and its natural and anthropogenic causes. J. Geophys. Res.-Atmos. 121, 3519–3533. https://doi.org/10.1002/2015JD024549.

Makowski, K., Jaeger, E.B., Chiacchio, M., Wild, M., Ewen, T., Ohmura, A., 2009. On the relationship between diurnal temperature range and surface solar radiation in Europe. J. Geophys. Res.-Atmos. 114, 1–16. https://doi.org/10.1029/2008J-D0111-04.

Nicholls, N., Alexander, L., 2007. Has the climate become more variable or extreme? Progress 1992-2006. Prog. Phys. Geogr. 31, 77–87. https://doi.org/10.1177/0309133307073885.

Pielke, Srmarland R.A., Betts, G., Chase, R.A., Eastman, T.N., Niles, J.L., 2002. The influence of land-use change and landscape dynamics on the climate system: relevance to climate-change policy beyond the radiative effect of greenhouse gases. Philos. Trans. 360, 1705. https://doi.org/10.1098/rsta.2002.1027.

Powell, E.J., Keim, B.D., 2014. Trends in daily temperature and precipitation extremes for the southeastern United States: 1948–2012. J. Clim. 28, 1592–1612. https://doi.org/10.1175/jcli-d-14-00410.1.

Ren, Y., Ren, G., 2011. A remote-sensing method of selecting reference stations for evaluating urbanization effect on surface air temperature trends. J. Clim. 24, 3179–3189. https://doi.org/10.1175/2010JCLI3658.1.

Ren, G., Zhou, Y., 2014. Urbanization effect on trends of extreme temperature indices of national stations over mainland China, 1961–2008. J. Clim. 27, 2340–2360. https://doi.org/10.1175/JCLI-D-13-00393.1.

Ren, G.Y., Chu, Z.Y., Chen, Z.H., Ren, Y.Y., 2007. Implications of temporal change in urban heat island intensity observed at Beijing and Wuhan stations. Geophys. Res. Lett. 34, 89–103. https://doi.org/10.1029/2006GL027927.

Ren, G., Zhou, Y., Chu, Z., Zhou, J., Zhang, A., Guo, J., Liu, X., 2008. Urbanization effects on observed surface air temperature trends in North China. J. Clim. 21, 1333–1348. https://doi.org/10.1175/2007JCLI1348.1.

Ren, G.Y., Zhang, A.Y., Chu, Z.Y., Zhou, J.X., Zhou, Y.Q., 2010. Principles and procedures for selecting reference surface air temperature stations in China. Meteor. Sci. Tech. 38, 78–85.

Ren, Y., Ren, G., Zhang, L., Zhou, Y., Zhang, A., 2015. An integrated procedure to determine a reference station network for evaluating and adjusting urban bias in surface air temperature data. J. Appl. Meteorol. Climatol. 54, 1248–1266. https://doi.org/10.1175/JAMC-D-14-0295.1.

Ren, C., Ren, G., Zhang, P., Tysa, S.K., Qin, Y., 2021. Urbanization significantly affects pan-evaporation trends in large river basins of China mainland. Land. 10 https://doi.org/10.3390/land10040407.

Rio, S.D., Cano-Ortiz, A., Herrero, L., Penas, A., 2012. Recent trends in mean maximum and minimum air temperatures over Spain (1961-2006). Theoret. Appl. Climatol. 109, 605–626. https://doi.org/10.1007/s00704-012-0593-2.

Romanov, P., 1999. Urban influence on cloud cover estimated from satellite data. Atmos. Environ. 3324, 4163–4172. https://doi.org/10.1002/pmic.200500182.

Stone, D.A., Weaver, A.J., 2003. Factors contributing to diurnal temperature range trends in twentieth and twenty-first century simulations of the coupled model. Clim. Dyn. 20, 435–445. https://doi.org/10.1007/s00382-002-0288-y.

Sun, X., Ren, G., Xu, W., Li, Q., Ren, Y., 2017. Global land-surface air temperature change based on the new CMA GLSAT data set. Sci. Bull. 62, 236–238. https://doi.org/10.1016/j.scib.2017.01.017.

Sun, X., Ren, G., You, Q., Ren, Y., Xu, W., Xue, X., 2018. Global diurnal temperature range changes since 1901. Clim. Dyn. 52, 3343–3356. https://doi.org/10.1007/s00382-018-4329-6.

Sun, X., Wang, C., Ren, G., 2021. Changes of diurnal temperature range over East Asia from 1901 to 2018 and its relationship with precipitation. Clim. Chang. 166 https://doi.org/10.21203/rs.3.rs-411321/v1.

Thorne, P.W., Donat, M.G., Dunn, R.J.H., Rennie, J.J., 2016. Reassessing changes in diurnal temperature range: inter comparison and evaluation of existing global data set estimates. J. Geophys. Res. 121, 5138–5158.

Tysa, S.K., Ren, G., Qin, Y., Zhang, P., Ren, Y., Jia, W., 2019. Urbanization effect in regional temperature series based on a remote sensing classification scheme of stations. J. Geophys. Res.-Atmos. 124 https://doi.org/10.1029/2019JD030948.

Varquez, A.C.G., Kanda, M., 2018. Global urban climatology: a meta-analysis of air temperature trends (1960–2009). Nat. Partn. J. Clim. Atmos. Sci. 32 https://doi.org/10.1038/s41612-018-0042-8.

Wang, K., Ye, H., Chen, F., Xiong, Y., Li, X., 2010. Long-term change of solar radiation in southeastern China: Variation, factors, and climate forcing. Ecol. Environ. Sci. 19, 6 (in Chinese). https://doi.org/10.1016/S1872-5813(11)60001-7.

Wang, H., Hao, Z., Zheng, J., 2014. Temporal and spatial distribution characteristics of strong volcanic eruption in 1750–2010. Acta Geograph. Sin. 69, 134–140 (in Chinese). https://doi.org/10.1007/s11442-014-1138-7.

Wild, M., 2012. Enlightening global dimming and brightening. Bull. Am. Meteorol. Soc. 93, 27–37. https://doi.org/10.1175/BAMS-D-11-00074.1.

Yang, S., Shi, G.Y., Wang, B., Yang, H., Duan, Y., 2013. Trends in Surface Solar Radiation (SSR) and the effect of clouds on SSR during 1961−2009 in China. Chin. J. Atmos. Sci. 37, 963–970 (in Chinese).

Yang, P., Ren, G.Y., Yan, P.C., Deng, J.M., 2021. Urbanization reduces frequency of light rain: an example from Beijing city. Theor. Appl. Climatol. 145, 763–774. https://doi.org/10.1007/s00704-021-03655-4.

Yin, H., Sun, Y., 2019. Characteristics of ESAT and precipitation in China in 2017 based on ETCCDI indices. Clim. Change Res. 15, 363–373. https://doi.org/10.1016/j.accre.2019.01.001.

Zhai, P., Pan, X., 2003. Trends in temperature extremes during 1951–1999 in China. Geophys. Res. Lett. 30, 169–172. https://doi.org/10.1029/2003GL018004.

Zhai, P.M., Zhou, B.Q., Chen, Y., 2021. Several new understandings in the climate change science. Clim. Change Res. 17 https://doi.org/10.12006/j.issn.1673-1719.2021.201.

Zhang, X., Vincent, L., Hogg, W., 2000. Temperature and precipitation trends in Canada during the 20th century. Atmosphere. 38, 395–429. https://doi.org/10.1080/07055900.2000.9649654.

Zhang, A.Y., Ren, G.Y., Zhou, J.X., Chu, Z., Tang, G., 2010. On the urbanization effect on surface air temperature trends over China. Acta Meteorl. Sin. 68, 957–966 (in Chinese).

Zhang, P., Ren, G., Qin, Y., Zhai, Y., Sun, X., 2021. Urbanization effects on estimates of global trends in mean and extreme air temperature. J. Clim. 34, 1923–1945. https://doi.org/10.1175/JCLI-D-20-0389.1.

Zhao, T.B., 2014. Correlation between atmospheric water vapor and diurnal temperature range over China. Atmosph. Oceanic Sci. Lett. 7, 369–375. https://doi.org/10.3878/j.issn.1674-2834.14.0005.

Zhao, N., Liu, S., Du, H., Yu, H., 2012. The effect of urbanization on sunshine duration and the trend of cloud cover amount variation in Beijing area. Climatic and Environmental. Research. 17, 233–243 (in Chinese). https://doi.org/10.3878/j.issn.1006-9585.2011.10140.